

## Scientific paper

# A Raman Study of the Sulfated Cement Hydrates: Ettringite and Monosulfoaluminate

Guillaume Renaudin, Rachid Segni, Dorota Mentel, Jean-Marie Nedelec, Fabrice Leroux and Christine Taviot-Gueho

Received 22 June 2007, accepted 16 September 2007

## Abstract

Ettringite (the AFt  $\text{Ca}_6\text{Al}_2(\text{OH})_{12}(\text{SO}_4)_3 \cdot 26\text{H}_2\text{O}$  compound) and monosulfoaluminate (the AFm  $\text{Ca}_4\text{Al}_2(\text{OH})_{12} \cdot \text{SO}_4 \cdot 6\text{H}_2\text{O}$  compound) phases were synthesised by the coprecipitation method and studied by micro-Raman spectroscopy. Hydrogen bond network, involving sulfate anions, ensures the cohesion of the structure of these two compounds; the columnar structure of ettringite as well as the lamellar structure of monosulfoaluminate. Raman spectroscopy has been used as a probe to investigate mainly the inter-columnar and the inter-lamellar regions of the structures. Raman spectra allowed the characterization of the local environment of sulfate anions and the hydrogen bond networks. A significant asset brought by Raman spectroscopy is the ability to work on hydrated cement products without specific sample preparation; *i.e.* without a risk to damage these hydrated compounds. Several examples of the possibilities brought by Raman spectroscopy in cement chemistry are given in this paper. A space group redetermination of the ettringite structure was performed on the basis of the point symmetry of sulfate tetrahedra. The inter-columnar region of ettringite was compared to the inter-lamellar region of monosulfoaluminate as these two structural parts contain the same species. The thermal behaviors at the beginning of the dehydration (up to 390 K) and the iron substitution in ettringite were also investigated.

## 1. Introduction

Up to now only few Raman spectroscopic studies have been performed in cement chemistry as reported in the reviews published by Ghosh and Handoo (1980), Bensted (1999), Potgieter-Vermaak *et al.* (2006) and Skibsted and Hall (2007). Bensted was the pioneer in using Raman spectroscopy (1976a) to characterize cement minerals, following by Conjeaud and Boyer (1980). Most of the papers devoted to the application of Raman spectroscopy in cement chemistry concerns the characterization of clinker anhydrous minerals (Bensted, 1976a – Conjeaud and Boyer, 1980 – Newman *et al.*, 2005), identification of the various calcium sulfate forms: gypsum  $\text{CaSO}_4 \cdot 2\text{H}_2\text{O}$ , bassanite  $\text{CaSO}_4 \cdot \frac{1}{2}\text{H}_2\text{O}$  and anhydrite  $\text{CaSO}_4$  (Bensted, 1976b – Prasad, 2001), study of cement hydration by recording the decrease in intensity of the signals from the anhydrous silicate phases (Tarrida *et al.*, 1995) and the effects of carbonation (Bensted, 1977 – Martinez-Ramirez, 2003). However some studies report the use of Raman spectroscopy to investigate cementitious hydrates: namely to distinguish thaumasite  $\text{Ca}_6\text{Si}_2(\text{OH})_{12}(\text{CO}_3)_2(\text{SO}_4)_2 \cdot 24\text{H}_2\text{O}$  from ettringite  $\text{Ca}_6\text{Al}_2(\text{OH})_{12}(\text{SO}_4)_3 \cdot 26\text{H}_2\text{O}$ , (Brough and Atkinson, 2001 – Jallad *et al.*, 2001 – Sahu *et al.*,

2002) and to characterize the C-S-H, calcium silicate hydrate, phase (Kirkpatrick *et al.*, 1997). The last two years there has been an increasing interest in applying Raman analyses on wet hydrating samples as mentioned by Skibsted and Hall (2007) and indicating by the numerous recent literature: hydration/carbonation of aluminate phases (Black *et al.*, 2006a and 2006b), silicate phases (Ibanez *et al.*, 2007), portlandite (El-Turki *et al.*, 2007) and cement (Martinez-Ramirez *et al.*, 2006 – Gastaldi *et al.*, 2007), structural features of C-S-H (Garbev *et al.*, 2007 – Black *et al.*, 2007), corrosion (Poupart *et al.*, 2006) and sulfate-attack (Ma *et al.*, 2006) of concrete. The aim of our study was to use the well known sulfated hydrated cementitious materials (ettringite and monosulfoaluminate  $\text{Ca}_4\text{Al}_2(\text{OH})_{12} \cdot \text{SO}_4 \cdot 6\text{H}_2\text{O}$ ) to explore the possibilities given by Raman spectroscopy. Not only the Raman shifts were examined, but also the band broadening (*i.e.* the Full Width at Half Maximum, FWHM) and the band profile fitting procedures associated with the corresponding irreducible representations. Raman spectroscopy has been used to reinvestigate the real space group of ettringite (as two models were proposed in 1968; one trigonal  $P31c$  model by Moore and Taylor, and one hexagonal  $P\bar{6}2c$  model by Courtois *et al.*) and to characterize its hydrogen bond network which assumes the cohesion between the columns of the structure. Our results are in perfect agreement with the recent definitive structural characterization made by Hartman and Berliner (2006) by Rietveld refinement on a neutron diffraction pattern from a deuterated ettringite sample. The sulfate local environment, the octahedral Al vibration and the hydrogen bond network (of great im-

portance in these hydrates) were compared in ettringite and in monosulfoaluminate. The effects of heat treatment and the effects of iron substitution were also investigated by Raman spectroscopy. These examples of local environment information brought by Raman spectroscopy combined with previously reported information on long-range order from X-ray diffraction allowed us to achieve a sharp description of the studied materials namely in the case of disordered compounds as the AFm phases (in which the crystallographic description of the interlayer region shows a statistical occupancies disorder combined sometimes with an orientation disorder).

## 2. Methods and materials

### 2.1 Samples syntheses

The compounds were prepared by the coprecipitation method at controlled pH. All syntheses were performed at room temperature with deionized decarbonated water under inert nitrogen atmosphere in order to avoid contamination by  $\text{CO}_3^{2-}$  ions. Typically, 10 mL of a mixed solution of  $\text{CaCl}_2$  0.66M and  $\text{M}^{3+}\text{Cl}_3$  0.33M was added dropwise to a reactor filled with 250 mL of 0.08M  $\text{Na}_2\text{SO}_4$  solution; the pH was kept constant at  $11.5 \pm 0.1$  by the simultaneous addition of 2.0 M NaOH solution. After complete addition of the metallic salts, the precipitate was aged in the mother solution for 24 hours. The crystallites were isolated by two centrifugation cycles in water then dried at room temperature under dynamic vacuum and finally stored in a  $\text{CO}_2$ -free atmosphere.

Two commercial products have been used to validate the profile fitting procedure on Raman spectra: gypsum ( $\text{CaSO}_4 \cdot 2\text{H}_2\text{O}$ , Merk, for analysis, purity > 99%) and thenardite ( $\text{Na}_2\text{SO}_4$ , Prolabo, normapur, purity > 99.9%). These two sulfate containing products were chosen because of their well known crystallographic structures and local sulfate environments.

### 2.2 Raman spectroscopy

Micro-Raman spectra were recorded at room temperature in the back scattering geometry, using a Jobin-Yvon T64000 device. The spectral resolution obtained with an excitation source at 514.5 nm (argon ion laser line, Spectra Physics 2017) is about  $1 \text{ cm}^{-1}$ . The Raman detector is a charge coupled device (CCD) multichannel detector cooled by liquid nitrogen to 140 K. The laser beam was focused onto the sample through an Olympus confocal microscope with x100 magnification. Laser spot was about  $1 \mu\text{m}^2$ . Measured power at the sample level was kept less than 15 mW (and less than 5 mW in cases of iron substituted samples) in order to avoid any damage to the material. The Raman scattered light was collected with the microscope objective at  $180^\circ$  from the excitation and filtered with an holographic Notch filter before being dispersed by a single grating (1800 grooves per mm). Several spectra were recorded (by accumulating ten spectra of 120s each) at different

points for the same sample in order to evaluate the homogeneity of the samples and the reproducibility of the main spectral features. Spectra were analyzed by using the profile fitting procedure with a Lorentzian function of the program *SPECTRAW* (Lovy, 1996). Spectra were recorded over the frequency ranges  $200 \text{ cm}^{-1} - 1300 \text{ cm}^{-1}$  and  $2800 \text{ cm}^{-1} - 4000 \text{ cm}^{-1}$  in order to investigate respectively the four Raman active vibration modes of sulfate anions, the ' $\text{Al}(\text{OH})_6$ ' octahedron vibration and the hydrogen bond network due to the water and hydroxyl symmetric stretching.

### 2.3 Powder X-rays diffraction

Powder X-ray diffraction patterns were recorded on a X'Pert Pro Philips diffractometer equipped with a PW3011/20 proportional detector and using  $\text{Cu K}\alpha$  radiation. Powder patterns were recorded at room temperature in the diffraction interval  $2^\circ < 2\theta < 80^\circ$ , with a step size of  $\Delta 2\theta = 0.03^\circ$  and a counting time of 15 s per step. Powder pattern were analyzed by Rietveld refinement with *FullProf* (Rodriguez-Carvajal, 2005). Refined lattice parameters of the synthesized samples were  $a = 11.254$  (1) Å and  $c = 21.488$  (4) Å ( $P31c$  space group) for ettringite, and  $a = 5.7609$  (7) Å and  $c = 26.828$  (2) Å for monosulfoaluminate sample. Lattice parameters of monosulfoaluminate correspond to the usually named AFm-12 phase (taken into account the effective water content in the interlayer part of the structure, by comparison with AFm-14 and AFm-16) according to ICDD pattern N° 45-0158. The two samples were single-phase.

## 3. Results and discussion

### 3.1 Hexagonal or trigonal structure of ettringite revisited by Raman spectroscopy

Crystal structure of ettringite,  $\text{Ca}_6\text{Al}_2(\text{OH})_{12} \cdot (\text{SO}_4)_3 \cdot 26\text{H}_2\text{O}$ , has been subject of controversy as one hexagonal  $P\bar{6}2c$  model was proposed by Courtois *et al.* (1968) and one trigonal  $P31c$  model was proposed by Moore and Taylor (1968, 1970). These two models were an improvement of the first single-crystal X-ray study performed by Bannister *et al.* in 1936 leading to a hexagonal  $P6_3/mmc$  description. Moore and Taylor (1968, 1970) attributed the hexagonal  $P\bar{6}2c$  description of ettringite to twinning and gave a  $P6_3/mcm$  average description in a pseudo-cell with a half  $\bar{c}/2$  parameter. The main difference between the trigonal  $P31c$  and the hexagonal  $P\bar{6}2c$  models is the number of independent crystallographic sites for the sulfate anions: two independent  $\text{SO}_4^{2-}$  tetrahedra with two different multiplicity factors due to a statistical occupation disorder in the hexagonal description, or a fully ordered trigonal description with three independent  $\text{SO}_4^{2-}$  tetrahedra which have the same multiplicity factor. Distinguishing the two models by X-ray diffraction is quite impossible without ambiguity. Then, the aim of this first part of the present work was to use Raman spectroscopy as a probe of local environment and point

symmetry of sulfate groups to determine the real symmetry of ettringite. Recently a neutron powder diffraction investigation on deuterated ettringite has been published by Hartman and Berliner (2006). Their Rietveld refinement led to the definitive fully ordered trigonal  $P31c$  description of ettringite structure in perfect agreement with our spectroscopic results presented below. Raman spectra have been measured with a high counting rate in order to allow high quality line fitting. **Figure 1** shows the recorded spectrum of ettringite with the assignments. Among the previously published Raman spectra of ettringite, those from Jallad *et al.* (2001), Sahu *et al.* (2002), Deb *et al.* (2003) and Black *et al.* (2006a and 2006b) are similar to our data, contrary to the first reported spectra on ettringite by Myneni *et al.* (1998) that differs significantly. Myneni *et al.* (1998) indicated three bands for the sulfate  $\nu_1$  mode with a large split about  $30\text{ cm}^{-1}$ . Only their  $\nu_1$  band at  $989\text{ cm}^{-1}$  corresponds to our observation, while their supplementary components are close to the  $\nu_1$  frequencies observed for gypsum, bassanite, anhydrite and free solvated sulfate (respectively 1004, 1013, 1012 and  $980\text{ cm}^{-1}$  according to Myneni *et al.*, 1998).

### 3.1.1 The vibration modes of sulfate anion

Point symmetry of sulfate anion was probed to investigate the space group of ettringite. **Table 1** gives the correlation diagrams for internal vibration of  $\text{SO}_4$  tetrahedra in the proposed hexagonal  $P\bar{6}2c$  and trigonal  $P31c$  descriptions. Correlation diagram corresponding to the

hexagonal  $P6_3/mcm$  average model is also indicated, as well as the two reference materials (gypsum and thenardite) used to validate the method. The three proposed models for ettringite give the same irreducible representation of the internal  $\text{SO}_4^{2-}$  vibrations. In all cases the point symmetry of  $\text{SO}_4$  tetrahedra is  $C_3$ . This is evident in the  $P\bar{6}2c$  and  $P31c$  (respectively  $D_{3h}^4$  and  $C_{3v}^2$ ) cases. In the case of the  $P6_3/mcm$  ( $D_{6h}^3$ ) average model, the actual  $D_3$  point symmetry becomes  $C_3$  when removing the mirror plane normal to the  $\bar{c}$  axis. The incompatible  $D_3$  point symmetry for the tetrahedral sulfate ion is due to its orientation disorder along the  $\bar{c}$  axis (see **Fig. 1** in Moore and Taylor, 1970). Removing the  $m$  mirror normal to  $\bar{c}$  implies an effective  $C_3$  point symmetry for  $\text{SO}_4$  tetrahedra. According to the  $C_3$  point symmetry, the  $\nu_1$  and  $\nu_2$  modes are not split. The  $\nu_3$  and  $\nu_4$  modes degenerate into two components  $\nu_3, \nu_3'$  and  $\nu_4, \nu_4'$ , respectively. In **Fig. 1** the  $\nu_3'$  and  $\nu_4'$  components are not mentioned because of the unresolved splitting of both  $\nu_3$  and  $\nu_4$  modes on the Raman spectrum. Probably the band broadening masks the presence of the two components. This irreducible representation agreed well with our observed Raman spectrum and with all the previously published works. Only the assignment given by Deb *et al.* (2003), with two components for the  $\nu_2$  mode (i.e. at  $416\text{ cm}^{-1}$  and  $449\text{ cm}^{-1}$ ), is in discrepancy. However they studied an ettringite from a natural source. The splitting they mentioned for the sulfate  $\nu_2$  mode and for the ' $\text{Al}(\text{OH})_6$ ' vibration can be attributed to the presence of cationic

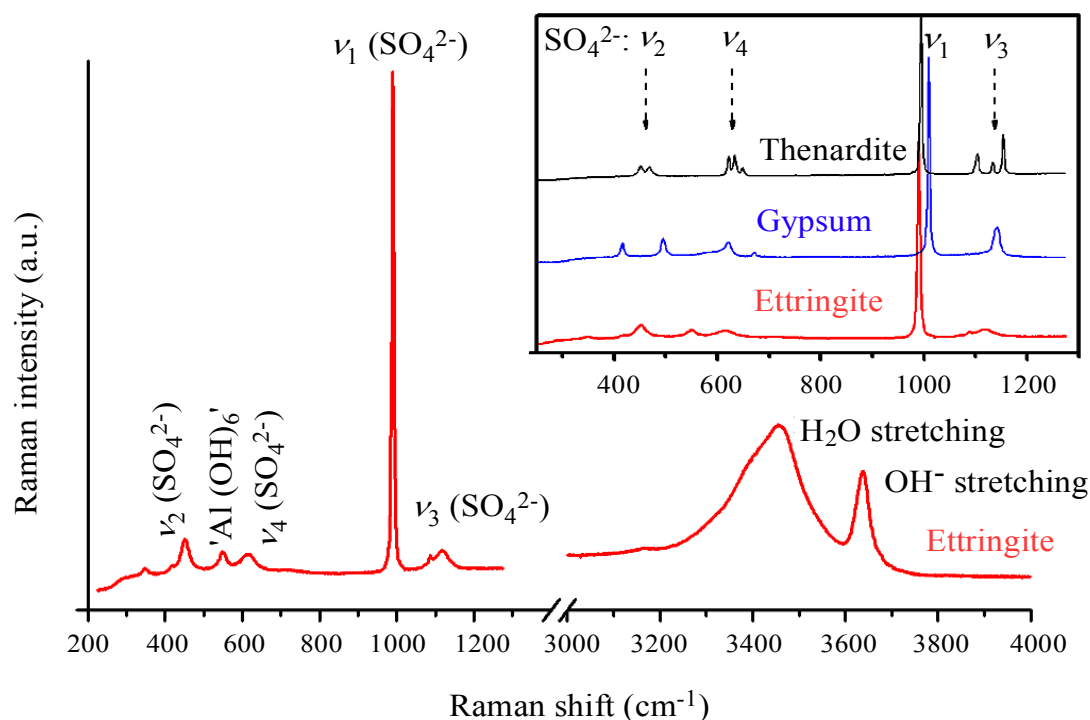


Fig. 1 Main window: Raman spectra of ettringite in the ranges  $200\text{ cm}^{-1} - 1300\text{ cm}^{-1}$  and  $3000\text{ cm}^{-1} - 4000\text{ cm}^{-1}$  recorded at room temperature. Inset window: Raman sulfate modes of vibration in ettringite (red; bottom), gypsum (blue; middle) and thenardite (black; top).

and anionic substitutions in their natural sample. The irreducible representations of the reference materials we used (gypsum and thenardite) are different from ettringite. In gypsum, the point symmetry of sulfate is  $C_2$ , leading to the splitting of the  $\nu_2$ ,  $\nu_3$  and  $\nu_4$  modes into two  $\nu_2$  and  $\nu_2'$  components, three  $\nu_3$ ,  $\nu_3'$  and  $\nu_3''$  components and three  $\nu_4$ ,  $\nu_4'$  and  $\nu_4''$  components respectively. The sulfate anion in thenardite, with the point symmetry  $D_2$ , showed the same splitting as gypsum (Table 1). As can be seen in the inset of Fig. 1, split modes were perfectly resolved in the case of thenardite: one band for  $\nu_1$  mode, two bands for  $\nu_2$  mode, three bands for  $\nu_3$  and  $\nu_4$  modes. In the case of gypsum the splitting of the  $\nu_2$  mode was about  $80\text{ cm}^{-1}$ , while the splitting of the  $\nu_3$  and  $\nu_4$  modes was not resolved. In all cases the  $\nu_1$  mode was by far the less broad and particularly the more intense vibration. According to these experimental observations the  $\nu_1$  band has been chosen for the profile fitting procedure. The aim of the profile fitting was to find the number of components in this  $\nu_1$  band, which indicated the number of crystallographic independent sites in the structure: one for the  $P6_3/mcm$  average model, two for the  $P\bar{6}2c$  hexagonal model and three for the  $P31c$  trigonal model. The intensity ratio (*i.e.* surface ratio) of the different components should correspond to the number of sulfate anions in each crystallographic independent site (*i.e.* linked to the multiplicity and the occupancy factor of each independent site). The hexagonal  $P\bar{6}2c$  description leads to a ratio of 2/1 (due to the occupancy factors of 1 and  $1/2$  for the two sulfate sites having the same multiplicity factor). The trigonal  $P31c$  description leads to a ratio of 1/1/1 (due to the full occupancy of the three sulfate sites having the same multiplicity factor). In order to validate the method, the band corresponding to the  $\nu_1$  mode in the reference materials should be perfectly fitted by using a unique component due to a unique sulfate site in both gypsum (Boeyens and Ichharam, 2002) and thenardite (Rasmussen *et al.*, 1996) structures.

Figure 2 shows the profile fitting obtained for gypsum and thenardite by using a unique component; in agreement with the previously mentioned correlation diagrams. Figure 3 and Table 2 indicate the results of profile fitting of the  $\nu_1$  band for ettringite performed between  $970\text{ cm}^{-1}$  and  $1010\text{ cm}^{-1}$ . Clearly the use of a unique component, corresponding to the  $P6_3/mcm$  average model led to a bad fit due to an evident asymmetrical shape of the measured signal (Fig. 3, left). The use of a Voigt function was not justified. It allowed only an artificial improvement of the fit as the asymmetrical feature of the peak was independent of the introduction of a Gaussian contribution. The fit performed by using two components was quite acceptable although the apparent asymmetrical shape of the  $\nu_1$  band was not fully fitted (Fig. 3, middle). However the fitted surface ratio of 1/1.25 (Table 2) between the two components disagreed with the expected 1/2 ratio for the  $P\bar{6}2c$  hexagonal model. Results obtained by using three components indicated a perfect line fitting (Fig. 3, right) leading to a fitted surface ratio 1/1.07/1.16 (Table 2) close to the 1/1/1 ratio expected for the  $P31c$  trigonal model. This profile fitting procedure of Raman spectra indicates the actual structure of ettringite is given by the  $P31c$  trigonal description. Recent works of Hartmann and Berliner (2006) led to the same conclusion. They performed a Rietveld refinement on powder neutron diffraction pattern from deuterated ettringite with the  $P31c$  trigonal description allowing the localisation of hydrogen (deuterium) positions. Their recent neutron diffraction study gave a direct indication of the trigonal symmetry of ettringite and validates our Raman spectroscopic method. The similarities observed between the three  $\nu_1$  components, *i.e.* Raman shift and FWHM (Table 2), is also in agreement with their structural description including the hydrogen bond network description. Indeed this means that the three crystallographically independent sulfate anions have a similar environment

Table 1 Correlation diagrams for internal vibrations of  $\text{SO}_4$  tetrahedra in the different structural models for ettringite, and in the two used reference materials (gypsum and thenardite):

| Fundamental modes | Site symmetry |                                      |  |                                  |                                  |                                     |
|-------------------|---------------|--------------------------------------|--|----------------------------------|----------------------------------|-------------------------------------|
|                   | Free ion      | Ettringite                           |  |                                  | Gypsum                           | Thenardite                          |
|                   |               | $P6_3/mcm$<br>$\rightarrow D_{6h}^3$ | $P\bar{6}2c$<br>$\rightarrow D_{3h}^4$ | $P31c$<br>$\rightarrow C_{3v}^2$ | $C2/c$<br>$\rightarrow C_{2h}^6$ | $Fddd$<br>$\rightarrow D_{2h}^{24}$ |
|                   | $T_d$         | $C_3^*$<br>1 site                    | $C_3$<br>2 sites                       | $C_3$<br>3 sites                 | $C_2$<br>1 site                  | $D_2$<br>1 site                     |
| $\nu_1$           | $A_1$         | A                                    | A                                      | A                                | A                                | A                                   |
| $\nu_2$           | E             | E                                    | E                                      | E                                | 2A                               | 2A                                  |
| $\nu_3$           | $T_2$         | A+E                                  | A+E                                    | A+E                              | A+2B                             | $A_1+A_2+A_3$                       |
| $\nu_4$           | $T_2$         | A+E                                  | A+E                                    | A+E                              | A+2B                             | $A_1+A_2+A_3$                       |

\* point symmetry  $D_3$  with an orientation disorder due to the mirror normal to  $\bar{C}$  axis lead to an effective site symmetry  $C_3$  for the sulfate tetrahedron.

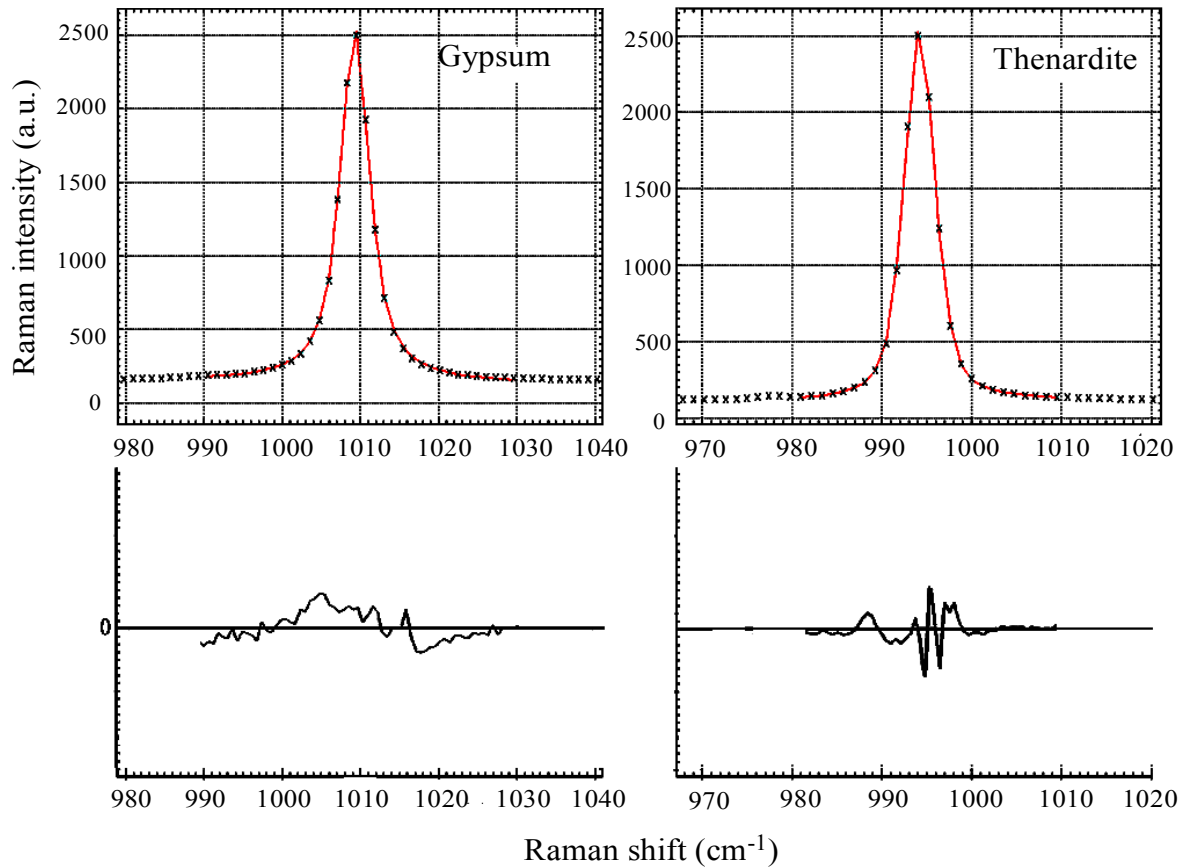


Fig. 2 Profile fitting (red curves) of  $\nu_1$  mode in measured Raman spectra (black crosses) performed by using a unique component for gypsum (left) and thenardite (right). Difference curves are plotted below (black line).

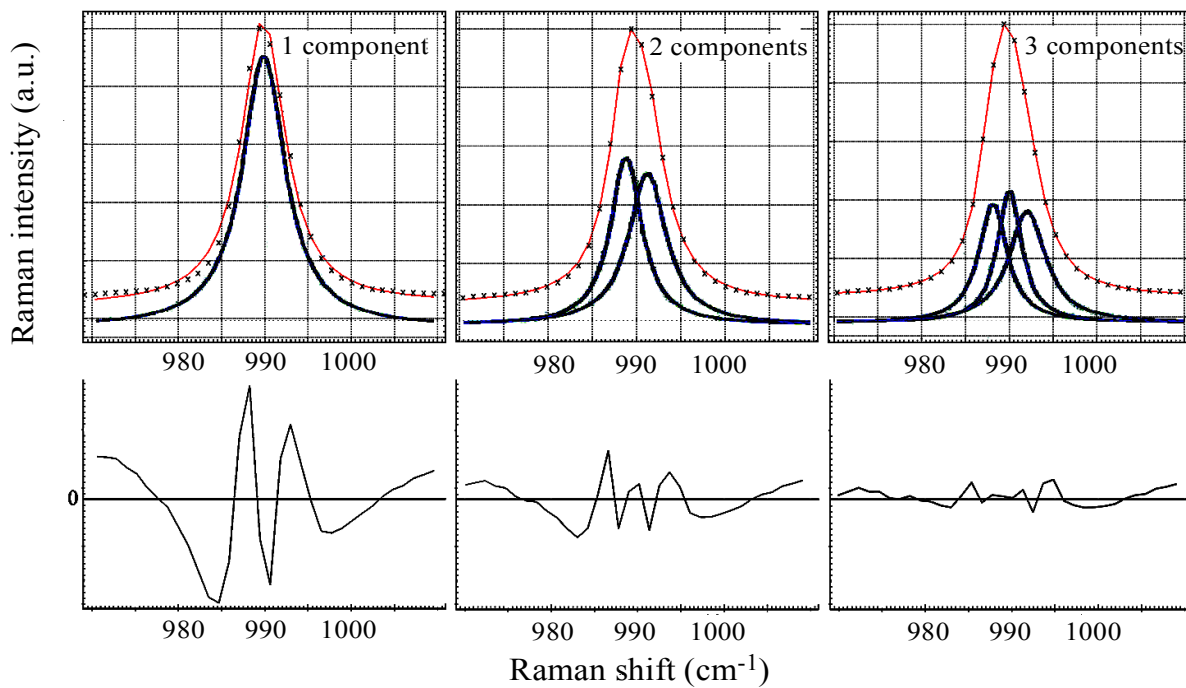


Fig.3 Profile fitting (red curves) of sulfate  $\nu_1$  mode from ettringite Raman spectra (black crosses) performed by using one (left), two (middle) and three (right) components. Fitted components are plotted in bold blue lines, and difference curves are plotted below (black line).

and only weak differences in the interatomic bond distances (sulfate to water distances) are observed. Each sulfate is neighbored by twelve hydrogen atoms belonging to twelve linked water molecules.

### 3.1.2 The hydrogen bond network vibrations

Micro-Raman spectra recorded in the range  $2800\text{ cm}^{-1}$  –  $4000\text{ cm}^{-1}$  were used to investigate the hydrogen bond network. **Figure 4** shows the fit performed over this frequency range. The spectrum was mainly composed by a broad band centred at  $3440\text{ cm}^{-1}$  (FWHM of  $173\text{ cm}^{-1}$ ) attributed to the water symmetric stretching mode and a sharper signal centred at  $3638\text{ cm}^{-1}$  (FWHM of  $33\text{ cm}^{-1}$ ) attributed to the hydroxyl symmetric stretching mode. The main features of the spectrum and the attri-

bution agreed with those from Deb *et al.* (2003) and Black *et al.* (2006b). A third weak band was observed at  $3165\text{ cm}^{-1}$  (FWHM of  $30\text{ cm}^{-1}$ ). Two shoulders at  $3300\text{ cm}^{-1}$  and  $3400\text{ cm}^{-1}$  were observed on the broad vibration band of water molecules. The different components of this broad signal were attributed to the presence of different kinds of water (free and bound) in ettringite as mentioned by Black *et al.* (2006b). The empirical Falk law (Falk, 1975) can be used to deduce the lengths of the hydrogen bonds (oxygen hydrogen bond donor to oxygen hydrogen bond acceptor interatomic distances) from the position of its corresponding stretching vibration. In the following Falk law  $\Delta\bar{\nu}$  is the Raman shift of the stretching band and  $r$  is the hydrogen bond length:

Table 2 Profile fitting results of sulfate  $\nu_1$  mode from Raman spectra.

| Sample     | number of components | Raman shift ( $\text{cm}^{-1}$ ) | FWHM* ( $\text{cm}^{-1}$ ) | Surface area (a.u.) | Surface ratio |
|------------|----------------------|----------------------------------|----------------------------|---------------------|---------------|
| Gypsum     | 1                    | 1009                             | 4.54                       | $1.56 \cdot 10^5$   | -             |
| Thenardite | 1                    | 994                              | 4.12                       | $1.28 \cdot 10^5$   | -             |
| Ettringite | 1                    | 990                              | 6.12                       | $2.37 \cdot 10^5$   | -             |
|            | 2                    | 989                              | 4.28                       | $0.96 \cdot 10^5$   | 1/1.25        |
|            |                      | 991                              | 5.40                       | $1.21 \cdot 10^5$   |               |
|            | 3                    | 988                              | 3.80                       | $0.61 \cdot 10^5$   | 1/1.07/1.16   |
| 990        |                      | 3.46                             | $0.65 \cdot 10^5$          |                     |               |
|            |                      | 992                              | 4.74                       | $0.71 \cdot 10^5$   |               |

\* Full Width at Half Maximum.

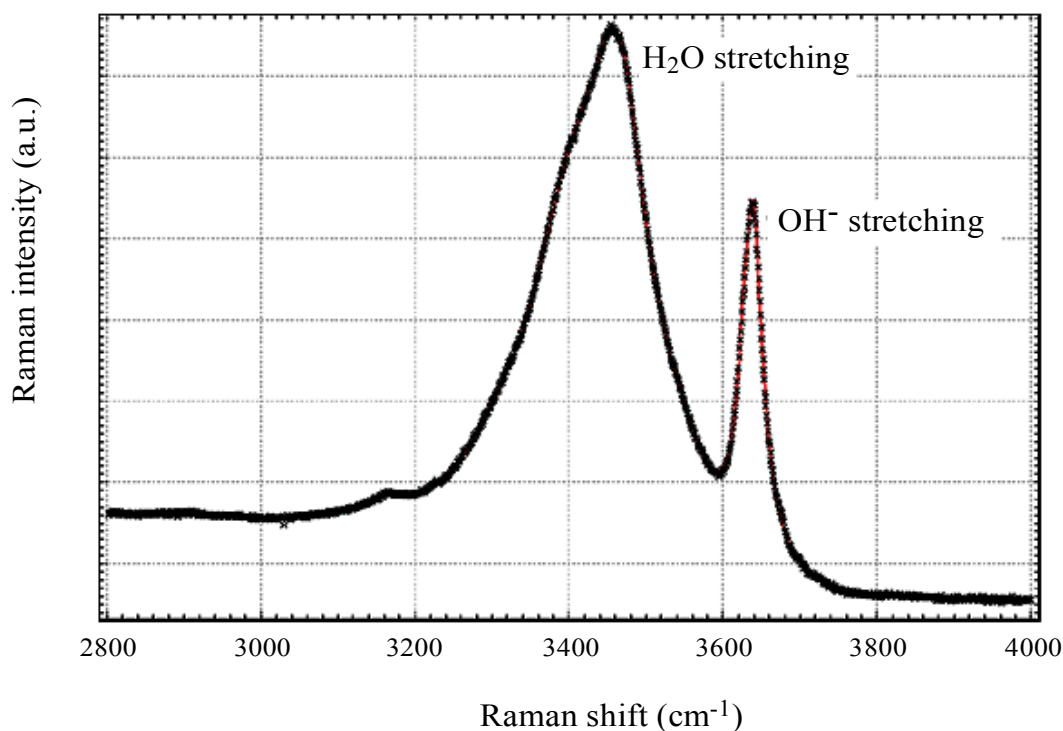


Fig. 4 Profile fitting (red curve) of the measured Raman spectra (black crosses) in the range  $2800\text{ cm}^{-1}$  -  $4000\text{ cm}^{-1}$  corresponding to the stretching of the hydrogen bonds in ettringite.

$$\Delta \bar{\nu} = 3707 - \frac{3707}{2727} \exp(20.96 - 5.539 r) \quad (1)$$

The hydroxyl band centered at  $3638 \text{ cm}^{-1}$  has been deconvoluted by bands ranging from  $3626 \text{ cm}^{-1}$  to  $3652 \text{ cm}^{-1}$  corresponding to hydrogen bond lengths from  $3.05 \text{ \AA}$  to  $3.12 \text{ \AA}$ . The broad band can be deconvoluted into several bands ranging from  $3303 \text{ cm}^{-1}$  to  $3544 \text{ cm}^{-1}$  corresponding to hydrogen bond lengths from  $2.76 \text{ \AA}$  to  $2.92 \text{ \AA}$ . While the weak band at  $3165 \text{ cm}^{-1}$  involved a hydrogen bond length of  $2.70 \text{ \AA}$ . Applying a systematic uncertainty about  $0.1 \text{ \AA}$  to these calculated interatomic distances (due to the simplicity of the model used that supposes linear hydrogen bonds) we can assumed that hydrogen bonds from hydroxyl anions, and water molecules respectively, have to be attributed for oxygen-oxygen distances  $2.95 \text{ \AA} < d_{\text{OH-O}} < 3.22 \text{ \AA}$ , and  $2.60 \text{ \AA} < d_{\text{H}_2\text{O-O}} < 3.02 \text{ \AA}$  respectively. To be considered as a possible acceptor the neighboring oxygen atom cannot participate to the same aluminum or calcium coordination polyhedron as the donor. In **Table 3** are gathered all these informations: the neighboring, the possibility to form a hydrogen bond and the inter-oxygen distances according to Moore and Taylor (1970) and Hartman and Berliner (2006). Our Raman study on water and hydroxyl stretching allowed us to identify the hydrogen bonds in the structure without knowing the hydrogen positions. The hydrogen bond network deduced from our spectroscopic study correspondes exactly to that solved by Hartman and Berliner (2006). The only missing hydrogen bond in our study was O12-H12a---O10 (atom labels were taken from Hartman and Berliner, 2006) because of its weakness as indicated by the large inter-oxygen distance of  $3.12 \text{ \AA}$  which was excluded from our  $2.60 \text{ \AA} < d_{\text{H}_2\text{O-O}} < 3.02 \text{ \AA}$  range. A discrepancy can also be observed on the O19 free water molecule. That can be easily attributed to its half site occupancy. In case of statistical disorder the refined interatomic distances can be artificially decreased and this can explains the short O19-H19b---O19 hydrogen bond obtained ( $d_{\text{O19-O19}} = 2.37 \text{ \AA}$ ). Such an inter-oxygen distance should lead to a stretching band around  $2940 \text{ cm}^{-1}$ . Raman spectroscopy enables a full description of the hydrogen bond network. The hydroxyl groups involve intra-columnar hydrogen bonds, along the  $[\text{Ca}_3\text{Al}(\text{OH})_6(\text{H}_2\text{O})_{12}]^{3+}$  columns. While linked water molecules involve two kinds of hydrogen bonds; a small part (i.e. one eighth) is intra-columnar perpendicular to the columns, the others seven eighths give the inter-columnar cohesion through sulfate anions and free water molecules.

### 3.2 Comparison of the Raman spectrum of ettringite and monosulfoaluminate

Raman spectroscopy is an adequate tool to compare the local environment of sulfate anion and the hydrogen bond networks in ettringite and monosulfoaluminate; *i.e.* to compare the inter-columnar part of the former with the inter-lamellar part of the latter. **Figure 5** shows the

Raman spectra from both cementitious sulfated phases (ettringite and monosulfoaluminate AFm-12). The spectrum from the monosulfoaluminate sample agrees with that from Black *et al.* (2006a and 2006b); in which the  $\nu_1$  mode was indicated at  $981 \text{ cm}^{-1}$  when hydrating pure  $\text{C}_3\text{A}$  in presence of sulfate (compared with our observation at  $982 \text{ cm}^{-1}$ , **Table 4**).

Raman spectra recorded on monosulfoaluminate in the range  $200 \text{ cm}^{-1} - 1300 \text{ cm}^{-1}$  show great similarity with the ettringite spectrum (**Fig. 5a**). We observed the four active modes of sulfate anion and the vibration of 'Al(OH)<sub>6</sub>' octahedron. In spite of the different structural features of ettringite and monosulfoaluminate, *i.e.* respectively a columnar and a lamellar structure, Raman spectra were quite similar in this frequencies range. **Table 4** gives the Raman frequencies and the full width at half maximum of the vibration bands. A shift of about  $17 \text{ cm}^{-1}$  was observed for the 'Al(OH)<sub>6</sub>' vibration which is attributed to the different environments. Al(OH)<sub>6</sub> octahedra are edge sharing with six in plane seven-fold coordinated calcium atoms (Ca(OH)<sub>6</sub>H<sub>2</sub>O polyhedron) in monosulfoaluminate compounds (Allmann, 1977). While Al(OH)<sub>6</sub> octahedra are edge sharing with six eight-fold coordinated calcium atoms (Ca(OH)<sub>4</sub>(H<sub>2</sub>O)<sub>4</sub> polyhedron) with three above and three under each Al(OH)<sub>6</sub> octahedron. These different neighbouring for Al atoms (see insets in **Fig. 5a**) lead to different Al—OH bonds constants resulting from the shift of the 'Al(OH)<sub>6</sub>' vibration frequency. Shifts were also observed for the sulfate symmetric stretching ( $\nu_1$  mode) and bending ( $\nu_3$  mode) although the asymmetric modes ( $\nu_2$  and  $\nu_4$ ) were not. The shift observed for the symmetric modes has to be attributed to sulfate anions lying in the different hydrogen bond networks. In the case of ettringite assuming the inter-column cohesion through sulfate anion the hydrogen bond network is well defined. In comparison, the hydrogen bond network in monosulfoaluminate is more flexible, namely due to a statistical occupancy disorder (between sulfate anion and free water molecules) and an orientation disorder of sulfate tetrahedron in the interlayer part of the structure. The presence of strong hydrogen bonds involving oxygen atoms from sulfate groups delocalized the electronic density from the anion resulting in a shift of the vibration frequency. The large FWHM observed for the  $\nu_1$  mode in monosulfoaluminate must also be attributed to the disorder in the interlayer region. The important splitting of the  $\nu_3$  and  $\nu_3'$  components (about  $60 \text{ cm}^{-1}$  for monosulfoaluminate compared to a splitting of about  $30 \text{ cm}^{-1}$  in case of ettringite) could not be explained in terms of local symmetry as point symmetry for sulfate is  $\text{C}_3$  in both monosulfoaluminate and ettringite structures. Yet these sulfate anions cannot be considered as similar since in monosulfoaluminate an apical oxygen atom from sulfate anion is directed to main layers and is chemically different to the three other basal oxygen atoms located close to the centre of the interlayer part. In the case of ettringite the four oxygen atoms from sulfate

Table 3 Hydrogen bonds interpretation to the profile fitting results of the Raman spectra in the range 2800 cm<sup>-1</sup> - 4000 cm<sup>-1</sup> in ettringite.

| Donor<br>O-H <sup>a</sup> | O<br>Neighbour <sup>b</sup> | Possible<br>acceptor<br>H---O <sup>c</sup> | Hydrogen bond<br>length O-H---O |                  | Hydrogen bonds <sup>e</sup> |
|---------------------------|-----------------------------|--|---------------------------------|------------------|-----------------------------|
|                           |                             |  | <sup>d</sup> (Å)                | <sup>e</sup> (Å) |                             |
| Hydroxyls:                |                             |  |                                 |                  |                             |
| O1                        | O3                          | -  | 3.07                            | 2.98             | O1-H1---O5                  |
|                           | O12                         | -  | 3.08                            | 3.06             |                             |
|                           | O10                         | -  | 3.11                            | 3.09             |                             |
|                           | O5                          | Yes  | 3.19                            | 3.27             |                             |
| O2                        | O9                          | -  | 2.94                            | 3.04             | O2-H2---O6                  |
|                           | O4                          | -  | 3.03                            | 3.02             |                             |
|                           | O11                         | -  | 3.07                            | 3.27             |                             |
|                           | O6                          | Yes  | 3.17                            | 3.06             |                             |
|                           | O5                          | -  | 3.39                            | 3.21             |                             |
| O3                        | O12                         | -  | 2.94                            | 2.96             | O3-H3---O7                  |
|                           | O10                         | -  | 2.95                            | 3.04             |                             |
|                           | O1                          | -  | 3.07                            | 3.07             |                             |
|                           | O7                          | Yes  | 3.22                            | 3.25             |                             |
| O4                        | O2                          | -  | 3.03                            | 3.04             | O4-H4---O8                  |
|                           | O8                          | Yes  | 3.12                            | 3.10             |                             |
|                           | O11                         | -  | 3.12                            | 2.93             |                             |
|                           | O9                          | -  | 3.24                            | 3.00             |                             |
| Linked water:             |                             |  |                                 |                  |                             |
| O5                        | O18                         | Yes  | 2.82                            | 2.79             | O5-H5a---O18                |
|                           | O16                         | Yes  | 2.98                            | 2.85             | O5-H5b---O16                |
| O6                        | O18                         | Yes  | 2.65                            | 2.70             | O6-H6b---O18                |
|                           | O16                         | Yes  | 2.70                            | 2.70             | O6-H6a---O16                |
|                           | O10                         | -  | 3.08                            | 2.99             |                             |
| O7                        | O17                         | Yes  | 2.77                            | 2.95             | O7-H7b---O17                |
|                           | O19                         | Yes  | 3.06                            | 2.88             | O7-H7a---O19                |
|                           | O11                         | -  | 3.10                            | 2.92             |                             |
| O8                        | O19                         | Yes  | 2.50                            | 2.64             | O8-H8a---O19                |
|                           | O17                         | Yes  | 2.83                            | 2.80             | O8-H8b---O17                |
|                           | O12                         | -  | 2.91                            | 2.95             |                             |
| O9                        | O16                         | Yes  | 2.60                            | 2.81             | O9-H9b---O16                |
|                           | O17                         | Yes  | 2.82                            | 2.55             | O9-H9a---O17                |
|                           | O11                         | Yes  | 2.82                            | 2.85             | O11-H11a---O9               |
|                           | O2                          | -  | 2.94                            | 3.02             |                             |
|                           | O4                          | -  | 3.24                            | 3.00             |                             |
| O10                       | O14                         | Yes  | 2.90                            | 2.87             | O10-H10a---O14              |
|                           | O18                         | Yes  | 2.95                            | 2.87             | O10-H10b---O18              |
|                           | O3                          | -  | 2.95                            | 3.07             |                             |
|                           | O6                          | -  | 3.08                            | 2.99             |                             |
| O11                       | O9                          | Yes  | 2.82                            | 2.85             | O11-H11a---O9               |
|                           | O15                         | Yes  | 2.88                            | 2.90             | O11-H11b---O15              |
|                           | O19                         | Yes  | 2.94                            | 2.69             | O19-H19b---O11              |
|                           | O7                          | -  | 3.10                            | 2.92             |                             |
|                           | O4                          | -  | 3.12                            | 2.93             |                             |
| O12                       | O13                         | Yes  | 2.82                            | 2.76             | O12-H12b---O13              |
|                           | O8                          | -  | 2.91                            | 2.95             |                             |
|                           | O3                          | -  | 2.94                            | 3.04             |                             |
| Free water:               |                             |  |                                 |                  |                             |
| O19                       | O19                         | Yes  | 2.42                            | 2.37             | O19-H19b---O19              |
|                           | O8                          | Yes  | 2.50                            | 2.64             |                             |
|                           | O11                         | Yes  | 2.94                            | 2.69             | O19-H19b---O11              |
|                           | O7                          | Yes  | 3.06                            | 2.88             |                             |

<sup>a</sup> Atom labels are those from [6] and [1], <sup>b</sup> Considered neighbour oxygen atoms are those involving an interatomic distance in relation with Falk law calculation (i.e. 2.60 Å < d<sub>Donor-Acceptor</sub> < 3.05 Å for hydrogen bond from water molecule, and 2.95 Å < d<sub>Donor-Acceptor</sub> < 3.22 Å for hydrogen bond from hydroxyl), <sup>c</sup> Neighbour oxygen atom is considered as possible acceptor only if it does not belong to the same coordination sphere as the donor. <sup>d</sup> data from Moore and Taylor (1970), <sup>e</sup> data from Hartman and Berliner (2006).

are more similar, in correlation with the weak splitting observed for the two  $\nu_3$  and  $\nu_3'$  components. The  $\nu_1$  mode of sulfate anion in the spectrum of monosulfoaluminate shows a shoulder of weak intensity at  $991\text{ cm}^{-1}$  (in italic in **Table 4**) corresponding to the  $\nu_1$  mode frequency of sulfate in ettringite ( $990\text{ cm}^{-1}$ ).

The frequency range  $2800\text{ cm}^{-1} - 4000\text{ cm}^{-1}$  (**Fig. 5b**) shows clearly two different hydrogen bond networks. Contrary to the case of ettringite (see 3.1.2), the spectrum of monosulfoaluminate was less resolved with an extremely broad band from  $3100\text{ cm}^{-1}$  to  $3500\text{ cm}^{-1}$  corresponding to water stretching. This large unresolved broad band is a consequence of the two kinds of disorder (as mentioned above) within the interlayer part of the monosulfoaluminate structure. Hydroxyl stretching appears at higher frequencies in monosulfoaluminate ( $3688\text{ cm}^{-1}$ , close to the band at  $3678\text{ cm}^{-1}$  assigned to the  $\text{OH}^-$  stretch of AFm-14 by Black *et al.*, 2006b) which corresponds to weakest hydrogen bonds involving hydroxyl groups in monosulfoaluminate compared to ettringite. In these two compounds hydroxyl groups participate to different kinds of hydrogen bonds. Indeed in monosulfoaluminate, hydroxyls are linked to the interlayer region (free water molecules and sulfate anions) and participate to the cohesion of the lamellar structure. While in ettringite hydroxyls only make intra-columnar hydrogen bonding and the cohesion of the structure is ensured by the linked water molecules.

### 3.3 Thermal behavior of ettringite and monosulfoaluminate

The thermal behavior of both samples were investigated *ex-situ*. Samples were heated at 320 K (ettringite sample) and 390 K (ettringite and monosulfoaluminate

samples) for two hours. Raman spectra were measured at room temperature on the heat treated samples just after their cooling down. **Figure 6** shows the Raman spectra (identical with those shown by Deb *et al.*, 2003, from room temperature up to 338 K). Frequencies and FWHM of the vibrations are gathered in **Table 4**. The dehydration of ettringite was clearly observed in the frequencies range  $2800\text{ cm}^{-1} - 3800\text{ cm}^{-1}$  (**Fig. 6b**) by the progressive departure of water molecules (progressive loss of the water stretching mode centred around  $3440\text{ cm}^{-1}$  and persistence of the hydroxyl stretching mode centred around  $3640\text{ cm}^{-1}$ ). The dehydration, without dehydroxylation, of ettringite is also indicated in **Table 4** by the surface ratio of the water/hydroxyl stretching bands which decreases from 4.5 on the as synthesised sample to 2.8 on the sample treated at 320 K, and to 0.9 on the sample treated at 390 K. The persistence of the hydroxyl stretching mode is accompanied with a large increase of its FWHM (from  $33.2\text{ cm}^{-1}$  on the as synthesised samples to  $38.1\text{ cm}^{-1}$  and  $49.9\text{ cm}^{-1}$  on the heat treated samples at respectively 320 K and 390 K). This is a consequence of the collapse of the ettringite structure when water molecules are leaving the intercolumnar region. The disruption of the ettringite structure due to dehydration above 340 K, has been described by Shimada and Young (2001). The same interpretation can be made from the evolution of the sulfate vibration bands: a considerable broadening of the vibration accompanied the heat treatment. Indeed the frequency of the sulfate  $\nu_1$  mode is shifted toward high frequencies, indicating strongest internal S—O bonds (which means that to sulfate anions are less implicated in the hydrogen bonding). The spectrum from ettringite heat treated at 320 K shows two components for the  $\nu_1$  mode: one at

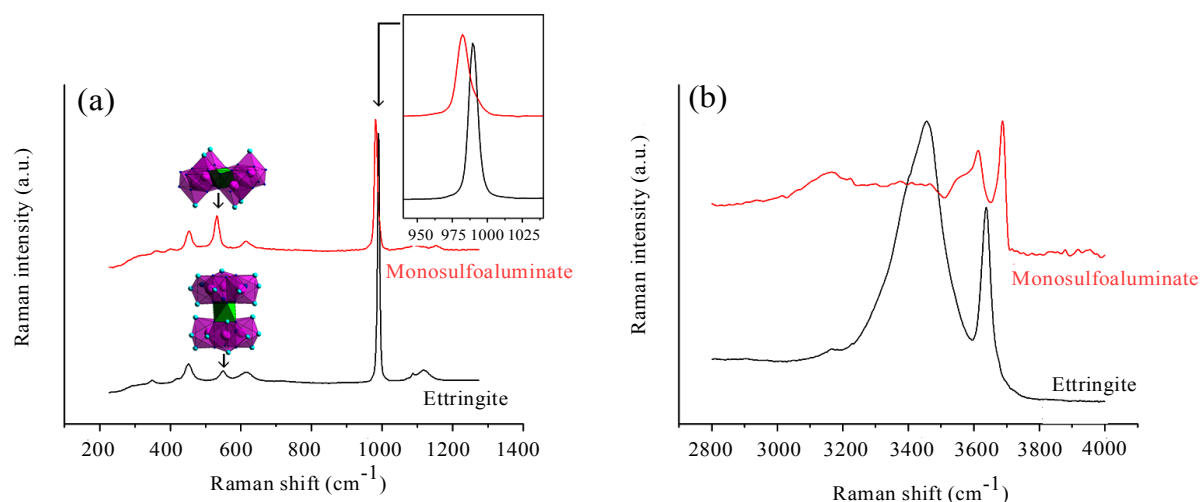


Fig. 5 Raman spectra on as synthesised ettringite (black curves) and monosulfoaluminate (red curves) in the frequencies ranges  $200\text{ cm}^{-1} - 1300\text{ cm}^{-1}$  (a: sulfate and ' $\text{Al}(\text{OH})_6$ ' vibrations) and  $2800\text{ cm}^{-1} - 4000\text{ cm}^{-1}$  (b: hydrogen bond stretching). In Figure 5a three insets show a zoom on the sulfate  $\nu_1$  mode (from  $940\text{ cm}^{-1}$  to  $1040\text{ cm}^{-1}$ ) and the neighbouring of  $\text{Al}(\text{OH})_6$  octahedron in ettringite and monosulfoaluminate structure (Al octahedron in green, Ca polyhedron in pink, water molecules and hydroxyls are respectively represented by light blue and small dark blue spheres).

Table 4 Raman frequencies ( $\text{cm}^{-1}$ ) and full width at half maximum ( $\text{cm}^{-1}$ ) of sulfate modes vibration, ' $\text{Al}(\text{OH})_6$ ' octahedron vibration and hydrogen bond stretching from ettringite and monosulfoaluminate in as synthesised samples and samples thermally treated at 320K and 390K.

|  | Ettringite     |             |              | Monosulfoaluminate       |                         |
|--|----------------|-------------|--------------|--------------------------|-------------------------|
|  | As synthesised | 320K        | 390K         | As synthesised           | 390K                    |
| $\nu_1$ sulfate mode                       |                |             |              |                          |                         |
| Raman shift                                | 990            | 988 / 1004  | 1003         | 982 / 991 <sup>Sh</sup>  | 980 <sup>Sh</sup> / 993 |
| FWHM (*)                                   | 6.2            | 11.6 / 27.8 | 33.70        | 7.4 / 10.2 <sup>Sh</sup> | 6.4 <sup>Sh</sup> / 6.0 |
| $\nu_2$ sulfate mode                       |                |             |              |                          |                         |
| Raman shift                                | 451            | 450         | 455          | 453                      | 452                     |
| FWHM (*)                                   | 24.6           | 46.8        | 70.2         | 18.8                     | 32.2                    |
| $\nu_3$ sulfate mode                       |                |             |              |                          |                         |
| Raman shift                                | 1087 / 1118    | 1123        | 1084 / 1147  | 1095 / 1154              | 1105                    |
| FWHM (*)                                   | 9.8 / 43.6     | 144.0       | 26.6 / 154.0 | 60.6 / 20.6              | 95.2                    |
| $\nu_4$ sulfate mode                       |                |             |              |                          |                         |
| Raman shift                                | 615            | 623         | 626          | 615                      | -                       |
| FWHM (*)                                   | 44.4           | 43          | 52.6         | 30.2                     | -                       |
| ' $\text{Al}(\text{OH})_6$ ' vibration     |                |             |              |                          |                         |
| Raman shift                                | 549            | 541         | 543          | 532                      | 532                     |
| FWHM (*)                                   | 21.0           | 32.8        | 42.0         | 15.0                     | 13.6                    |
| Water stretching                           |                |             |              |                          |                         |
| Raman shift                                | 3440           | 3455        | 3515         | -                        | -                       |
| FWHM (*)                                   | 173.4          | 298.8       | 209.0        | -                        | -                       |
| Hydroxyl stretching                        |                |             |              |                          |                         |
| Raman shift                                | 3638           | 3628        | 3621         | 3688                     | 3675                    |
| FWHM (*)                                   | 33.2           | 76.2        | 99.8         | 24.7                     | 24.6                    |
| Surface ratio (water band / hydroxyl band) |                |             |              |                          |                         |
| $\text{H}_2\text{O} / \text{OH}^-$         | 4.5            | 2.8         | 0.9          | -                        | -                       |

(\*) Full Width at Half Maximum.

<sup>Sh</sup> Shoulder of weak intensity.

988  $\text{cm}^{-1}$  (corresponding to the as synthesised sample) and another at 1004  $\text{cm}^{-1}$  (corresponding to the collapsed ettringite). The ettringite sample heat treated at 390 K showed only the  $\nu_1$  mode at 1003  $\text{cm}^{-1}$  (corresponding to the collapsed ettringite). These *ex-situ* measurements gave evidence that the collapse of the ettringite structure is initiated but remains reversible for a thermal dehydration at 320K, and becomes irreversible for a thermal dehydration at 390 K (as the component at 988  $\text{cm}^{-1}$  was not at all observed).

The case of monosulfoaluminate is different (Fig. 6c and 6d). In spite of a shift of the sulfate  $\nu_1$  mode (from 982  $\text{cm}^{-1}$  to 993  $\text{cm}^{-1}$ ) when heated at 390 K, the frequencies range 2800  $\text{cm}^{-1}$  – 4000  $\text{cm}^{-1}$  shows evidence of the presence of water molecules (by the extremely broad band from 3100  $\text{cm}^{-1}$  to 3600  $\text{cm}^{-1}$ ). Water molecules are still present in the heat treated monosulfoaluminate sample but the hydrogen bond stretching bands are modified compared to the as-synthesised sample (the shape of the extremely broad band related to water stretching is modified, and the position of the band of the hydroxyl stretching is shift to lower wavenumber; *i.e.* from 3688  $\text{cm}^{-1}$  to 3675  $\text{cm}^{-1}$ ). This could be attrib-

uted to a reconstruction phenomenon of the AFm phases (already mentioned in case of the nitrated AFm phase by Renaudin *et al.*, 2000), confirmed by the presence of the shoulder of the  $\nu_1$  mode at 980  $\text{cm}^{-1}$  corresponding to the as synthesised monosulfoaluminate phase. The collapse of the monosulfoaluminate structure when dehydrated does not take place at 390K as inferred by the absence of band broadening; the FWHM of the sulfate  $\nu_1$  mode of 7.4  $\text{cm}^{-1}$  on the as synthesised sample is about the same order (6.0  $\text{cm}^{-1}$ ) for the sample treated at 390 K. In the same way, vibration of the ' $\text{Al}(\text{OH})_6$ ' polyhedra, still active for monosulfoaluminate heat treated at 390 K, indicates the absence of disruption of the main layer in the AFm structure. In the case of the AFt phase, the ' $\text{Al}(\text{OH})_6$ ' vibration on sample heat treated at 390 K disappears in agreement with the  $^{27}\text{Al}$  NMR observation made by Shimada and Young, 2001 (change in the coordination number of aluminium from 6 to 4 in ettringite heat treated at 390 K).

### 3.4 Iron substitution in ettringite

The solid solution  $\text{Ca}_6(\text{Al}_{2-x}\text{Fe}_x)(\text{OH})_{12}\cdot(\text{SO}_4)_3\cdot 26\text{H}_2\text{O}$ , corresponding to the substitution of aluminium by iron

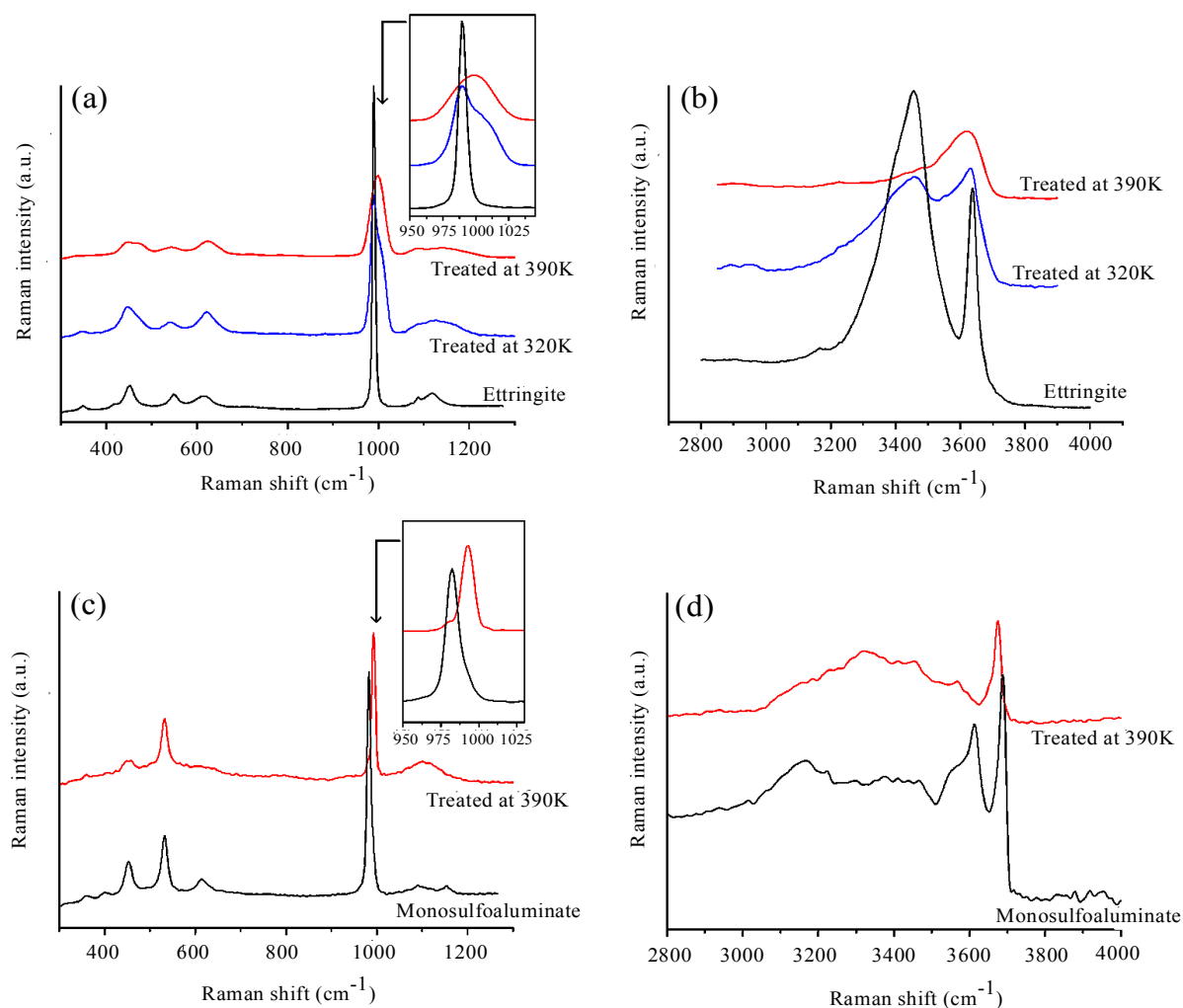


Fig. 6 Raman spectra on as synthesised (black curves) and thermally treated at 320 K (blue curves) and 390 K (red curves) samples of ettringite and monosulfoaluminate in the frequencies ranges  $200\text{ cm}^{-1} - 1300\text{ cm}^{-1}$  (a and c: sulfate and  $\text{Al}(\text{OH})_6$  vibrations for respectively ettringite and monosulfoaluminate samples) and  $2800\text{ cm}^{-1} - 4000\text{ cm}^{-1}$  (b and d: hydrogen bond stretching for respectively ettringite and monosulfoaluminate samples). Insets in Figure 6a and 6c show a zoom on the sulfate  $\nu_1$  mode (from  $950\text{ cm}^{-1}$  to  $1030\text{ cm}^{-1}$ ).

in ettringite, has also been investigated. The replacement of  $\text{Al}^{3+}$  by  $\text{Fe}^{3+}$  in ettringite structure has already been reported (Buhlert and Kuzel, 1971), as numerous other possible substitutions (Pöllmann *et al.*, 1989). We present in this paper (devoted to Raman use to characterize sulfated cementitious hydrates) only our main Raman spectroscopic results on this study. The complete study on the iron substitution in ettringite will be published elsewhere. **Figure 7** shows the frequency range corresponding to the sulfate and octahedral Al vibration. The indicated Al/Fe ratios correspond to the ratio of the mother solution during synthesis. Powder X-ray diffraction patterns indicated that samples were single-phase. **Figure 8** shows the Rietveld refinement, Profil Matching procedure with *FullProf* (Rodriguez-Carvajal, 2005), performed on the 50/50 substituted iron ettringite. The refined lattice parameters, indicated in **Table 5**, confirm that with increasing amounts of Fe in ettringite, there is

a progressive decrease of the  $a$  lattice parameter combined with a progressive increase of the  $c$  lattice parameter. The Raman spectra give evidence for the deterioration of the ettringite structure due to iron substitution. This deterioration was not observed on the X-ray diffraction patterns (as showing in **Fig. 8**). This indicates that the ettringite structure is not modified at the crystallite size, but at the sulfate molecular level: only the environment of the sulfate anions (*i.e.* the hydrogen bond network) is affected by the iron substitution. We observed a fall of the ettringite characteristic signal; only the  $\nu_1$  mode of sulfate was still clearly visible. The iron substitution led to a shift toward the high frequencies (from  $990\text{ cm}^{-1}$  in pure ettringite to  $1001\text{ cm}^{-1}$  in the 90/10 substituted ettringite, and to  $1008\text{ cm}^{-1}$  in the 50/50 substituted ettringite) and an increase of its FWHM (from  $6.2\text{ cm}^{-1}$  in pure ettringite to about  $40\text{ cm}^{-1}$  in the substituted ettringites). This shift to higher

wavenumber whit the iron substitution has not been observed by Black *et al.*, 2006a, during the hydration of  $C_4AF$  in presence of sulfate. They observed always the  $\nu_1$  sulfate band at  $989\text{ cm}^{-1}$ , but they have no indication for the presence of iron in their ettringite. We observed also a decrease in the water and hydroxyl stretching signals in the range  $2800\text{ cm}^{-1} - 4000\text{ cm}^{-1}$  (not shown here). Aluminium replacement by iron in ettringite led to the same spectroscopic observations made by thermal

treatment: a modification of the ettringite framework due to an apparent disruption of the hydrogen bond network.

#### 4. Conclusions

This paper shows several examples illustrating the abilities of Raman spectroscopy to study hydrated cementitious phases. An important aspect is the investigation of

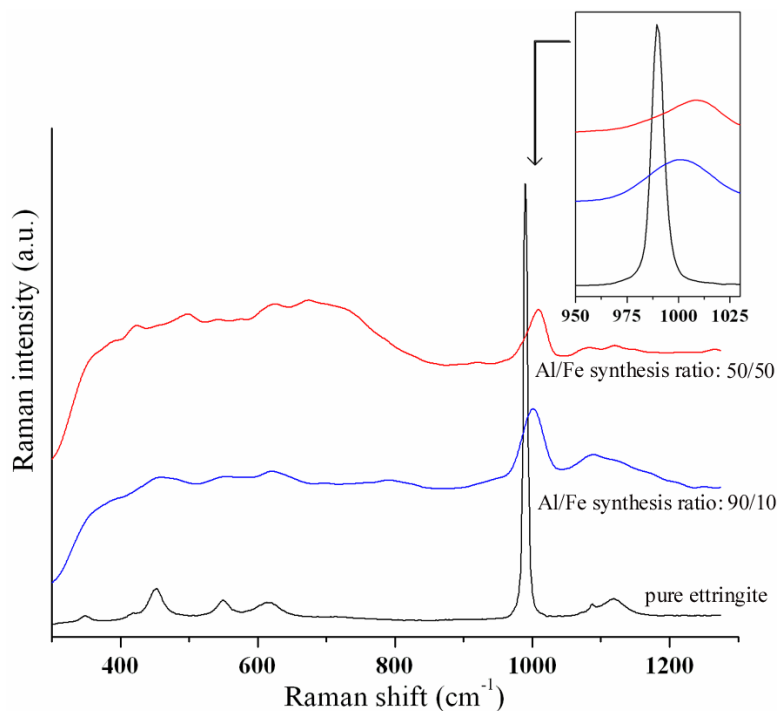


Fig. 7 Raman spectra on pure ettringite (black curve) and on iron substituted ettringite (introduced Al/Fe ratio in the synthesis mother solution of 90/10 and 50/50 for respectively the blue and red curves) samples in the frequencies ranges  $200\text{ cm}^{-1} - 1300\text{ cm}^{-1}$ . Insets show a zoom on the sulfate  $\nu_1$  mode (from  $950\text{ cm}^{-1}$  to  $1030\text{ cm}^{-1}$ ).

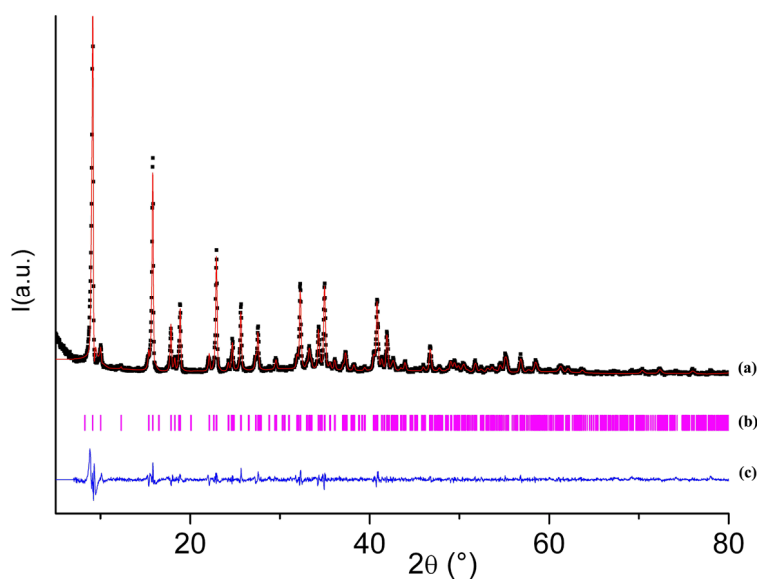


Fig. 8 Rietveld plot on the single phased 50/50 substituted iron ettringite sample: observed and calculated patterns (a: black dot squares and red line respectively), Bragg peaks positions (b) and difference curve (c).

Table 5 Refined lattice parameter of the different synthesized ettringite samples (pure and iron substituted) of composition  $\text{Ca}_6(\text{Al}_{2-x}\text{Fe}_x)(\text{OH})_{12}(\text{SO}_4)_3 \cdot 26\text{H}_2\text{O}$  using the trigonal  $P31c$  space group.

| Synthesis                         | Lattice parameters (Å)               |
|-----------------------------------|--------------------------------------|
| Pure ettringite                   | $a = 11.254$ (1)<br>$c = 21.488$ (4) |
| 90/10 iron substituted ettringite | $a = 11.249$ (4)<br>$c = 21.49$ (1)  |
| 50/50 iron substituted ettringite | $a = 11.240$ (9)<br>$c = 21.55$ (1)  |

the local environment of the anionic species and the hydrogen bond network through the measurement of the water and hydroxyl stretchings. The work shown here on sulfate anions can be performed on numerous polynuclear anions encountered in cement chemistry, such as carbonate, nitrate, chlorate, arseniate, chromate, phosphate, silicate, etc... The profile fitting procedure on a selected vibration provides information on point symmetry which can be used to complete and/or confirm structural studies (see part 3.1.1). The profile fitting of the broad bands in the range  $3000 \text{ cm}^{-1} - 4000 \text{ cm}^{-1}$  allows us to identify and localise the hydrogen bonds ensuring the structural cohesion of the hydrated phases (see part 3.1.2). The environment of a selected anion in different cementitious phases is also of interest (see part 3.2). Raman spectra on the heat treated samples provide information on the thermal behavior of the compounds: the deterioration of the hydrogen bond network, the modification of the anionic environment, and the collapse of the structural framework (see part 3.3). Effects due to cationic substitution can also be investigated by means of Raman spectroscopy (see part 3.4). The studies presented in this paper on single-phase samples can be carried out more complex cement systems allowing a deeper understanding of the underlying chemical mechanisms, as indicated by the increasing number of recent articles on this topic.

### Acknowledgements

D. M. would like to thank Erasmus network for its financial support.

### References

Allman, R. (1977). "Refinement of the hydrid layer structure  $\text{Ca}_2\text{Al}(\text{OH})_6 \cdot \frac{1}{2}\text{SO}_4 \cdot 3\text{H}_2\text{O}$ ." *Neues Jahrbuch für Mineralogie Monatshefte*, 217, 136-144.

Bannister, F. A., Hey, M. H. and Bernal, J. D. (1936). "Ettringite from Scawt Hill." *Mineralogical Magazine*, 24, 324-328.

Bensted, J. (1976a). "Uses of Raman spectroscopy in cement chemistry." *Journal of the American Ceramic Society*, 59 (3-4), 140-143.

Bensted, J. (1976b). "Appraisal of the calcium sulfate – water system by Raman spectroscopy." *Zement Kalk*

*Gips*, 29 (9), 416-418.

Bensted, J. (1977). "Raman spectral studies of carbonation phenomena." *Cement and Concrete Research*, 7 (2), 161-164.

Bensted, J. (1999). *Colloquium on Techniques for Characterization of Cement Hydration—New and Old Techniques*, Society of Chemical Industry Constructions Materials Group, London (1999).

Black, L., Breen, C., Yarwood, J., Deng, C.-S., Phipps, J. and Maitland, G. (2006a). "In situ Raman analysis of hydrating  $\text{C}_3\text{A}$  and  $\text{C}_4\text{AF}$  pastes in presence and absence of sulfate." *Advances in Applied Ceramics*, 1005 (4), 209-216.

Black, L., Breen, C., Yarwood, J., Deng, C.-S., Phipps, J. and Maitland, G. (2006b). "Hydration of tricalcium aluminate ( $\text{C}_3\text{A}$ ) in the presence and absence of gypsum – studied by Raman spectroscopy and X-ray diffraction." *Journal of Materials Chemistry*, 16, 1263-1272.

Black, L., Breen, C., Yarwood, J., Garbev, K., Stemmermann, P. and Gasharova, B. (2007). "Structural features of C-S-H (I) and its carbonation in air – A Raman spectroscopic study. Part II: Carbonated phases." *Journal of the American Ceramic Society*, 90 (3), 908-917.

Boeyens, J. C. A. and Icharam, V. V. H. (2002). "Redetermination of the crystal structure of calcium sulfate dihydrate,  $\text{CaSO}_4 \cdot 2\text{H}_2\text{O}$ ." *Zeitschrift fuer Kristallographie*, 217, 9-10.

Brough, A. R. and Atkinson, A. (2001). "Micro-Raman spectroscopy of thaumasite." *Cement and Concrete Research*, 31 (3), 421-424.

Conjeaud, M. and Boyer, H. (1980). "Some possibilities of Raman microprobe in cement chemistry." *Cement and Concrete Research*, 10 (1), 61-70.

Buhlert, R. and Kuzel, H.-J. (1971). "The replacement of  $\text{Al}^{3+}$  by  $\text{Cr}^{3+}$  and  $\text{Fe}^{3+}$  in ettringite." *Zement Kalk Gips*, 2, 83-85.

Courtois, A., Dusausoy, Y., Lafaille, A. and Protas, J. (1968). "Preliminary study of the crystal structure of ettringite." *Comptes rendus de l'Académie des Sciences de Paris - Série D*, 266 (19), 1911-1913. (in French)

Deb, S. K., Manghnani, M. H., Ross, K., Livingston, R. A. and Monteiro, P. J. M. (2003). "Raman scattering and X-ray diffraction study of the thermal decomposition of an ettringite-group crystal." *Physics and Chemistry of Minerals*, 30, 31-38.

El-Turki, A., Ball, R. J. and Allen, G. C. (2007). "The influence of relative humidity on structural and chemical changes during carbonation of hydraulic lime." *Cement and Concrete Research*, 37 (8), 1233-1240.

Falb, M. (1975). In: W. A. Adams Ed. *Chemistry and physics of aqueous gas solution*. Princeton: Electrochem. Soc. Inc., 19.

Garbev, K., Stemmermann, P., Black, L., Breen, C., Yarwood, J. and Gasharova, B. (2007). "Structural

- features of C-S-H (I) and its carbonation in air – A Raman spectroscopic study. Part I: Fresh phases.” *Journal of the American Ceramic Society*, 90 (3), 900-907.
- Gastaldi, D., Boccaleri, E., Canonico, F. and Bianchi, M. (2007). “The use of Raman spectroscopy as a versatile characterization tool for calcium sulfoaluminate cements: a compositional and hydration study.” *Journal of Materials Science*, 42 (20), 8426-8432.
- Ghosh, S. N. and Handoo, S. K. (1980). “Infrared and Raman spectral studies in cement and concrete (review).” *Cement and Concrete Research*, 10 (6), 771-782.
- Hartman, M. R. and Berliner, R. (2006). “Investigation of the structure of ettringite by time-of-flight neutron powder diffraction techniques.” *Cement and Concrete Research*, 36, 364-370.
- Ibanez, J., Artus, L., Cusco, R., Lopez, A., Menendez, E. and Andrade, M. C. (2007). “Hydration and carbonation of monoclinic C<sub>2</sub>S and C<sub>3</sub>S studied by Raman spectroscopy.” *Journal of Raman Spectroscopy*, 38 (1), 61-67.
- Jallad, K. N., Santhanam, M., Cohen, M. D. and Ben-Amotz, D. (2001). “Chemical mapping of thaumasite in sulfate-attacked cement mortar using near-infrared Raman imaging microscopy.” *Cement and Concrete Research*, 31 (6), 953-958.
- Kirkpatrick, R. J., Yarger, J. L., McMillan, P. F., Yu, P. and Cong, X. (1997). “Raman spectroscopy of C-S-H, Tobermorite, and Jennite.” *Advanced Cement Based Materials*, 5 (3-4), 93-99.
- Lovy, D. (1996). Program *SPECTRAW*, Version 1.40, Département de Chimie Physique, University of Geneva, Switzerland.
- Ma, B., Gao, X., Byars, E. A. and Zhou, Q. (2006). “Thaumasite formation in a tunnel of Bapanxia Dam in Western China.” *Cement and Concrete Research*, 36 (4), 716-722.
- Martinez-Ramirez, S., Sanchez-Cortes, S., Garcia-Ramos, J. V., Domingo, C., Fortes, C. And Blanco-Varela, M. T. (2003). “Micro-Raman spectroscopy applied to depth profiles of carbonates formed in lime mortar.” *Cement and Concrete Research*, 33 (12), 2063-2068.
- Martinez-Ramirez, S., Frias, M. and Domingo, C. (2006). “Micro-Raman spectroscopy in white portland cement hydration: long-term study at room temperature.” *Journal of Raman Spectroscopy*, 37 (5), 555-561.
- Moore, A. E. and Taylor, H. F. W. (1968). “Crystal structure of ettringite.” *Nature*, 218, 1048-1049.
- Moore, A. E. and Taylor, H. F. W. (1970). “Crystal structure of ettringite.” *Acta Crystallographica*, B26, 386-393.
- Myneny, S. C., Traina, S. J., Waychunas, G. A. and Logan, T. J. (1998). “Vibrational spectroscopy of functional group chemistry and arsenate coordination in ettringite.” *Geochimica and Cosmochimica Acta*, 62 (21-22), 3499-3514.
- Newman, S. P., Clifford, S. J., Coveney, P. V., Gupta, V., Blanchard, J. D., Serafin, F., Ben-Amotz, D. and Diamond, S. (2005). “Anomalous fluorescence in near-infrared Raman spectroscopy of cementitious materials.” *Cement and Concrete Research*, 35 (8), 1620-1628.
- Pöllmann, H., Kuzel, H.-J. and Wenad, R. (1989). “Compounds with ettringite structure.” *Neues Jahrbuch für Mineralogie Monatshefte*, 160 (2), 133-158.
- Potgieter-Vermaak, S. S., Potgieter, J. H. and Van Grieken R. (2006). “The application of Raman spectrometry to investigate and characterize cement, Part I: A review.” *Cement and Concrete Research*, 36(4), 656-662.
- Poupard, O., L’Hostis, V., Catinaud, S. and Petre-Lazar, I. (2006). “Corrosion damage diagnosis of a reinforced concrete beam after 40 years natural exposure in marine environment.” *Cement and Concrete Research*, 36(3), 504-520.
- Prasad, P. S. R., Pradhan, A. and Gowd, T. N. (2001). “In situ micro-Raman investigation of dehydration mechanism in natural gypsum.” *Current Science*, 80 (9), 1203-1207.
- Rasmussen, S. E., Jorgensen, J.-E. and Lundtoft, B. (1996). “Structure and phase transition of Na<sub>2</sub>SO<sub>4</sub>.” *Journal of Applied Crystallography*, 29, 42-47.
- Renaudin, G., Rapin, J.-P., Humbert, B. and François, M. (2000). “Thermal behavior of the nitrated AFm phase Ca<sub>4</sub>Al<sub>2</sub>(OH)<sub>12</sub>(NO<sub>3</sub>)<sub>2</sub>·4H<sub>2</sub>O and structure determination of the intermediate hydrate Ca<sub>4</sub>Al<sub>2</sub>(OH)<sub>12</sub>(NO<sub>3</sub>)<sub>2</sub>·2H<sub>2</sub>O.” *Cement and Concrete Research*, 30 (2), 307-314.
- Rodriguez-Carvajal, J. (2005). PROGRAM *FullProf.2k*, version 3.20, Laboratoire Léon Brillouin (CEA-CNRS), France, (*FullProf.2k* manual available on [http://www-llb.cea.fr/fullweb/fp2k/fp2k\\_divers.htm](http://www-llb.cea.fr/fullweb/fp2k/fp2k_divers.htm)).
- Sahu, S., Exline, D. L. and Nelson, M. P. (2002). “Identification of thaumasite in concrete by Raman chemical imaging.” *Cement and Concrete Composites*, 24 (3-4), 347-350.
- Shimada, Y. and Young, J. F. (2001). “Structural changes during thermal dehydration of ettringite.” *Advances in Cement Research*, 13 (2), 77-81.
- Skibsted, J. and Hall, C. (2007). “Characterization of cement minerals, cements and their reaction products at the atomic and nanoscale level.” In: J. J. Beaudoin, J. M. Makar and L. Raki, Eds. *12<sup>th</sup> International Congress on the Chemistry of Cement*, Montreal 8-13 July 2007.
- Tarrida, M., Madon, M., Le Rolland, B. and Colombet, P. (1995). “An in-situ Raman spectroscopy study of the hydration of tricalcium silicate.” *Advanced Cement Based Materials*, 2 (1), 15-20.